(Received 13 October 2023, Accepted 26 December 2023, Scheduled 5 January 2024)

An Active Flux Model-Based Sensorless Flux Weakening Control Algorithm for Permanent Magnet Synchronous Motors

Kun Li, Lin Wang, and Yilin Zhu*

Jiangsu Changjiang Intelligent Manufacturing Research Institute Co, Ltd., Changzhou 213001, China

ABSTRACT: In order to improve the stability of sensorless high-speed operation of permanent magnet synchronous motors and effectively expand the speed range, a voltage closed-loop flux weakening sensorless algorithm based on the active flux model is proposed. Firstly, the mathematical model of sensorless control of the PMSM is designed based on the active flux model, and the state of the PMSM flux weakening operation is analyzed. Then, based on the voltage closed-loop flux weakening control method, the corresponding flux weakening control algorithm is analyzed and designed. Meanwhile, based on the active flux model, the speed and rotor position of the motor are observed by sliding mode observer and phase-locked loop method. After that, the flux weakening control method and sensorless control method are combined to realize the sensorless flux weakening control method to improve the stability of the control system. Finally, the proposed algorithm is validated on the experimental platform. The experimental results show that the proposed method can prevent the system from losing control during flux weakening processes, effectively improve system stability, and have smaller angle errors. The speed convergence time is shortened by 80% compared to the non flux weakening control.

1. INTRODUCTION

Permanent magnet synchronous motors (PMSMs) are currently widely used in CNC machine tools, mainly because PMSMs have the characteristics of small heat generation, reliable operation, high power density, and simple structure [1, 2]. In CNC grinding machines, encoder-free PMSM is often used. In this application field, because the motor must be applied in high speed and harsh environments, the spindle motor of CNC grinding machines must have characteristics such as fast rotation speed, high-speed accuracy, and strong system robustness. The speed limit of traditional photoelectric encoders does not exceed 6500 r/min, and their anti-pollution ability is poor, so they are not suitable for the use in this application. Other devices such as rotary transformers and magnetic encoders have some shortcomings to some extent. Therefore, it is necessary to develop a sensorless control algorithm for high-speed applications [3, 4].

At present, according to the differences in PMSM application scenarios, sensorless control algorithms are mainly divided into low-speed and zero-speed sensorless control algorithms [6–10] and medium to high-speed sensorless control algorithms [11–13]. In low-speed and zero-speed sensorless control algorithms, the extraction of speed and position signals is mainly achieved by injecting high-frequency signals. However, this type of method is not applicable at medium to high speeds. The sensorless control algorithm at medium to high speeds is mainly based on the back electromotive force (EMF) model, which estimates the back EMF value through different types of observers to achieve observation of speed and rotor position. In the medium and high-speed sensorless control algorithms, there are mainly two types: based on the extended back EMF model [5, 6, 14–17] and based on the active flux model [18–22]. Ref. [5] proposes an improved model reference adaptive system (MRAS) method, which estimates stator resistance and permanent magnet flux in both reference and adjustable models to suppress the adverse effects of parameter changes on control performance, and continuously updates them. Then, the Grey Wolf Optimization algorithm is used to optimize the proportional integral controller parameters of the speed adaptive law obtained by MRAS. In [6], by applying the Quadratic Extended Back-Electromotive Force model and combining injection-based and model-based position estimation into a universal sensorless control strategy for full-speed operation, the switching problem of the motor from low-speed to high-speed sensorless control is solved. In [15], a sensorless magnetic field-oriented vector control strategy is proposed that combines an improved adaptive sliding mode observer and a back EMF observer. In this method, an adaptive sliding mode observer is used to obtain the error of the back EMF and reduce system chattering. Meanwhile, the back EMF observer can adaptively track the speed and position of the rotor, avoiding complex calculations. It has the characteristics of fast convergence, small chattering, and good robustness. In [16], a simple design guide and an adaptive full-order observer are proposed. This method is based on the extended back EMF model, and the adaptive law and feedback gain are designed in a cascade manner. At the same time, a high bandwidth state observer is studied to eliminate the impact of speed estimation errors on system stability, and an adaptive feedback loop is added to ensure good rotor speed estimation performance at lower frequencies. The extended back electromotive force model is the basis for [17], which offers a thorough analysis of sensorless control algorithms for sliding mode observers. It also suggests de-

* Corresponding author: Yilin Zhu (yl.zhu.dy@gmail.com).

signing SMOs in non-ideal scenarios and addresses potential directions for future research on sliding mode observer-based sensorless control techniques.

The sensorless control method based on the active flux model is first proposed in [18]. When being applied to high-saliency PMSM, this method can achieve full-speed domain operation without injecting signals and has good application value. An adaptive second-order active flux observer is introduced in [19] to monitor the active flux. An MRAS-based compensation strategy is suggested to account for voltage source inverter (VSI) nonlinearity, thereby minimizing observation errors in a variety of speed ranges. [20] uses an active flux model to cascade the natural velocity observer and active flux estimator, resulting in a simple sensorless algorithm that only needs to determine a bandwidth parameter for flux estimation and a frequency band parameter for velocity observation. In [21], a new frequency adaptive second-order disturbance observer is proposed using the active flux model for the estimation of back EMF and active flux. This method eliminates the need for a phase delay compensator for traditional sliding mode observer-based back EMF estimators. In addition, the active flux and back EMF are estimated simultaneously, so the rotational speed and rotor position can be identified using quadrature phase-locked loop and tan inverse method.

The above sensorless control methods based on entended EMF (EEMF) and active flux models have been widely studied. In CNC grinding machines, the required high-speed is essential, so flux weakening control is also particularly important. Sensorless flux weakening control based on the EEMF model has been explored [23, 24], while there is little research on sensorless flux weakening control based on the active flux model. Therefore, studying the sensorless flux weakening control algorithm based on the active flux model is of great significance for improving the high-speed operation performance of PMSM in CNC grinding machines. Therefore, the research focus of this article is on the sensorless flux weakening control method based on active flux. On the one hand, a sensorless control algorithm for PMSM is designed based on an active flux model. On the other hand, based on the voltage closed-loop flux weakening control method, flux weakening control is achieved. Combine the two to achieve a sensorless flux weakening control algorithm. This algorithm not only effectively improves the running speed of the motor, but also improves the stability during flux weakening operation.

2. MATHEMATICAL MODEL AND FLUX WEAKENING CONTROL ANALYSIS

2.1. Active Flux-based Model of PMSM

In the d-q rotation coordinate system, the mathematical model of PMSM is:

$$\begin{bmatrix} u_d \\ u_q \end{bmatrix} = \begin{bmatrix} R+pL_d & -\omega_e L_q \\ \omega_e L_d & R+pL_q \end{bmatrix} \begin{bmatrix} i_d \\ i_q \end{bmatrix} + \begin{bmatrix} 0 \\ \omega_e \lambda_f \end{bmatrix} \quad (1)$$

where the subscripts d and q respectively represent the coordinate axes corresponding to the rotating coordinate system. Therefore, i_d, i_q, L_d, L_q, u_d, and u_q are the current, inductance, and voltage components corresponding to the coordinate axis. R represents stator resistance, λ_f represents the flux linkage of permanent magnet, ω_e represents the rotor angular velocity value, and in surface mounted permanent magnet synchronous motors (SPMSMs), there exists $L_d = L_q = L_s$ because the d- and q-axis reluctances are equal.

After calculation, it can be obtained that:

$$\begin{bmatrix} u_d \\ u_q \end{bmatrix} = R \begin{bmatrix} i_d \\ i_q \end{bmatrix} + pL_q \begin{bmatrix} i_d \\ i_q \end{bmatrix} + \omega_e L_q \begin{bmatrix} -i_q \\ i_d \end{bmatrix} + \begin{bmatrix} \lambda'_{ex} \\ \omega_e \lambda_{ex} \end{bmatrix} \quad (2)$$

where λ_{ex} is the active flux. λ'_{ex} is the derivative of the active flux.

After coordinate transformation, it can be obtained that:

$$\begin{bmatrix} u_\alpha \\ u_\beta \end{bmatrix} = R \begin{bmatrix} i_\alpha \\ i_\beta \end{bmatrix} + pL_q \begin{bmatrix} i_\alpha \\ i_\beta \end{bmatrix} - \begin{bmatrix} \lambda'_{\alpha ex} \\ \lambda'_{\beta ex} \end{bmatrix} \quad (3)$$

where the subscripts α and β respectively represent the coordinate axes corresponding to the stationary coordinate system. Therefore, i_α, i_β, u_α, and u_β are the current, inductance, and voltage components corresponding to the coordinate axis. $\lambda'_{\alpha ex}$ and $\lambda'_{\beta ex}$ represent the components of λ'_{ex} on α- and β-axes.

$$\begin{bmatrix} \lambda_{\alpha ex} \\ \lambda_{\beta ex} \end{bmatrix} = \lambda_{ex} \begin{bmatrix} \cos\theta_e \\ \sin\theta_e \end{bmatrix} \quad (4)$$

After converting (3) into current vector form, it can be expressed as:

$$L_q \boldsymbol{i}'_{\boldsymbol{\alpha\beta}} = \boldsymbol{u}_{\boldsymbol{\alpha\beta}} - R\boldsymbol{i}'_{\boldsymbol{\alpha\beta}} - \boldsymbol{\lambda}'_{\boldsymbol{\alpha\beta} ex} \quad (5)$$

Compared with the traditional EEMF model, the active flux model has no cross-coupling term, does not rely on d-axis inductance, and has a permanent magnet magnetic flux. Therefore, the active flux model has better robustness to parameter changes and external load changes.

2.2. Mathematical Model of Motor Flux Weakening Control

When the motor is in a stable weak magnetic operation state, and the speed is high, the resistance voltage drop and current differential term in the winding can be ignored. Therefore, the voltage equation in a flux weakening state can be rewritten as:

$$\begin{bmatrix} u_d \\ u_q \end{bmatrix} = \begin{bmatrix} 0 & -\omega_e L_q \\ \omega_e L_d & 0 \end{bmatrix} \begin{bmatrix} i_d \\ i_q \end{bmatrix} + \begin{bmatrix} 0 \\ \omega_e \lambda_f \end{bmatrix} \quad (6)$$

Meanwhile, the voltage also meets the requirements:

$$u_d^2 + u_q^2 \le U_m^2 \quad (7)$$

where U_m is the maximum value of stator voltage.

Then, from Equation (6), it can be obtained that:

$$\frac{i_q^2}{\frac{U_m^2}{(\omega_e L_q)^2}} + \frac{(i_d + i_f)^2}{\frac{U_m^2}{(\omega_e L_d)^2}} \le 1 \quad (8)$$

The curve described in Equation (8) is an ellipse, and both the long axis and broken axis are functions related to speed.

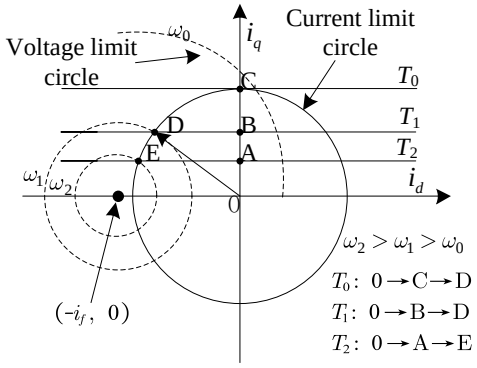

FIGURE 1. The trajectory of the current operating state.

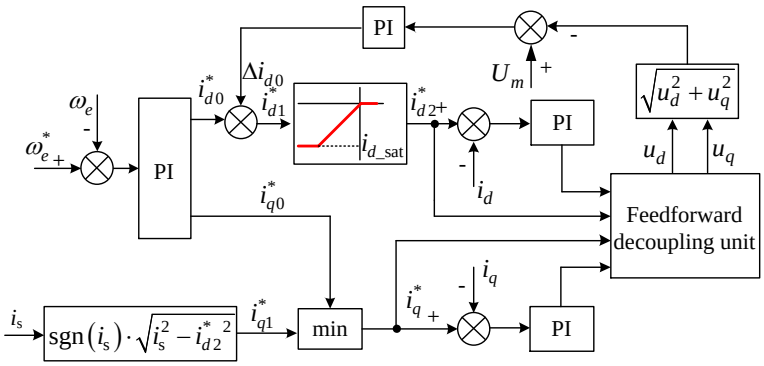

FIGURE 2. The block diagram of the voltage closed-loop flux weakening control.

Because the prototype used in this design is a surface-mounted PMSM with $L_d = L_q$, the curve described in the above equation is circular, and the center of the voltage circle corresponds to $(-i_f,\ 0)$. Meanwhile, according to the expression, as the speed increases, the voltage circular curve becomes a cluster of circular curves.

At the same time, the current also satisfies the following expression:

$$i_d^2 + i_q^2 \le I_m^2 \tag{9}$$

where I_m is the maximum value of stator current.

The curves corresponding to (8) and (9) are shown in Fig. 1. From Fig. 1, it can be seen that the center of the voltage circle $(-i_f, 0)$ is located outside the current limit circle. As the speed increases, the current i_q approaches 0, and (8) can be rewritten as:

$$(i_d + i_f)^2 \le \frac{U_m^2}{(\omega_e L_d)^2} \tag{10}$$

From (10), it can be seen that when $i_d \to i_f$, $\omega_e \to \infty$ and the rotor magnetic flux exceeds the maximum magnetic field provided by the stator current, the center of the circle depicted in Fig. 1 is outside the current limit circle. This characteristic of the motor will cause a sharp decrease in power when the speed exceeds the rated speed, indicating the existence of a theoretical maximum speed.

3. FLUX WEAKENING CONTROL METHOD AND SENSORLESS CONTROL METHOD

3.1. Theoretical Analysis of Flux Weakening Control Method

At present, the mainstream flux weakening control method is voltage closed-loop flux weakening control, and the implementation diagram of this method is shown in Fig. 2.

The voltage closed-loop control algorithm satisfies the following expression:

$$\begin{cases} u_s \ge U_m, & \Delta i_{d0} = f\left(U_m - u_s\right) \\ u_s < U_m, & \Delta i_{d0} = 0 \end{cases} \tag{11}$$

where $f(\cdot)$ represents the functional relationship corresponding to the proportional-integral (PI) controller.

In the control block diagram, due to the use of a limiting function, the output value of i^*_{d2} will always be 0 when $u_s < U_m$.

3.2. Design of Sliding Mode Observer and Phase-Locked Loop

Figure 3 shows the speed sensorless control block diagram of a sliding mode observer (SMO) based on active flux model.

In this design, a sliding mode surface is defined as:

$$\boldsymbol{s} = \boldsymbol{i}_{\alpha\beta} - \hat{\boldsymbol{i}}_{\alpha\beta} \tag{12}$$

The current observation equation can be written as:

$$L_q \hat{\boldsymbol{i}}'_{\boldsymbol{\alpha\beta}} = \boldsymbol{u}_{\boldsymbol{\alpha\beta}} - R\hat{\boldsymbol{i}}'_{\boldsymbol{\alpha\beta}} + k\mathrm{sgn}\left(\boldsymbol{s}\right) \tag{13}$$

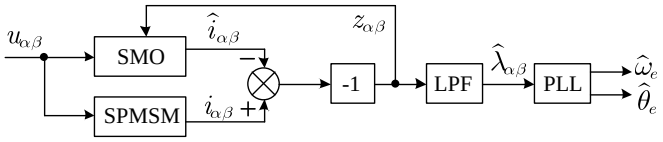

FIGURE 3. Speed sensorless control block diagram of a sliding mode observer.

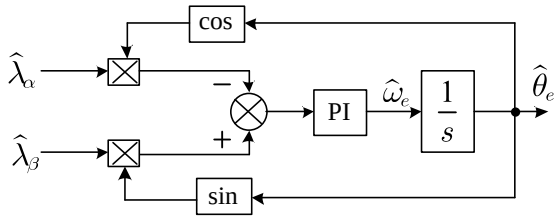

FIGURE 4. Block diagram of the phase-locked loop.

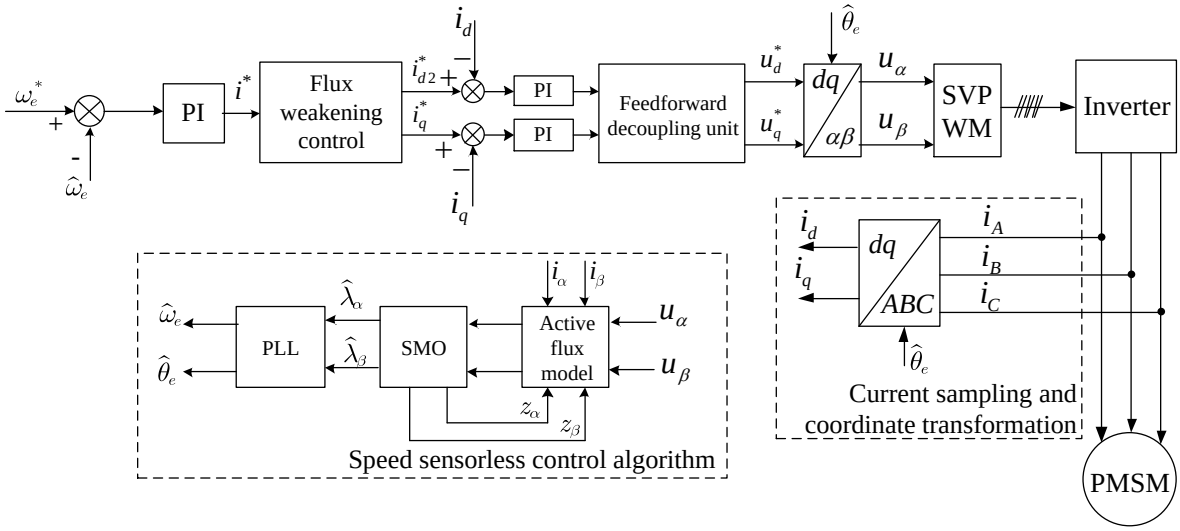

FIGURE 5. Block diagram of the sensorless flux weakening control algorithm.

where $\hat{\boldsymbol{i}}_{\boldsymbol{\alpha\beta}}$ represent the observed values of stator current.

Subtracting (13) from (5) yields:

$$L_q\tilde{\boldsymbol{i}}'_{\boldsymbol{\alpha\beta}} = -R\tilde{\boldsymbol{i}}'_{\boldsymbol{\alpha\beta}} - \boldsymbol{\lambda}'_{\boldsymbol{\alpha\beta}ex} - k\mathrm{sgn}(\boldsymbol{s}) \tag{14}$$

where $\tilde{\boldsymbol{i}}_{\boldsymbol{\alpha\beta}}$ represent the error values between actual stator current and observed stator current.

The stability of the system can be proven by the following Lyapunov function, which is defined as:

$$V = \frac{1}{2}s^2, V' = s \cdot s' = s \cdot \left(-R\tilde{\boldsymbol{i}}'_{\boldsymbol{\alpha\beta}} - \boldsymbol{\lambda}'_{\boldsymbol{\alpha\beta}ex} - k\mathrm{sgn}(\boldsymbol{s})\right) \tag{15}$$

When $s > 0$ and $V' < 0$, the system is asymptotically stable. When $s < 0$, in order to make $V' < 0$, it must be ensured that $k > \|\boldsymbol{\lambda}'_{\boldsymbol{\alpha\beta}ex}\|$. Equivalent control can be applied to sliding mode surfaces, and the back electromotive force satisfies $\boldsymbol{\lambda}'_{\boldsymbol{\alpha\beta}ex} = -k\mathrm{sgn}(\boldsymbol{s})$. After obtaining the flux derivative or back electromotive force through a sliding mode observer, the phase-locked loop (PLL) shown in Fig. 4 can be used to identify the speed and rotor position.

The basic principle of phase-locked loop satisfies:

$$\Delta E = -\lambda_{\alpha ex}\sin\hat{\theta}_e + \lambda_{\beta ex}\cos\hat{\theta}_e = \lambda_{ex}\sin\left(\theta_e - \hat{\theta}_e\right) \tag{16}$$

Adjust the error component obtained in (16) by PI controller to obtain the observed speed value $\hat{\omega}_e$. After integration, the observed rotor position value $\hat{\theta}_e$ can be obtained.

3.3. The Proposed Sensorless Flux Weakening Control Method

By combining the flux weakening control algorithm mentioned in Subsection 3.1 with the sensorless control algorithm mentioned in Subsection 3.2, a block diagram of the sensorless flux weakening control algorithm can be drawn as shown in Fig. 5. From Fig. 5, it can be seen that when the motor does not enter the flux weakening control state, sensorless control is carried out using the control method with $i_d = 0$. When the motor enters the flux weakening control state, the terminal voltage of the motor reaches a saturation state, and the motor achieves flux weakening control by increasing the d-axis current in the negative direction, and continuously performing sensorless control.

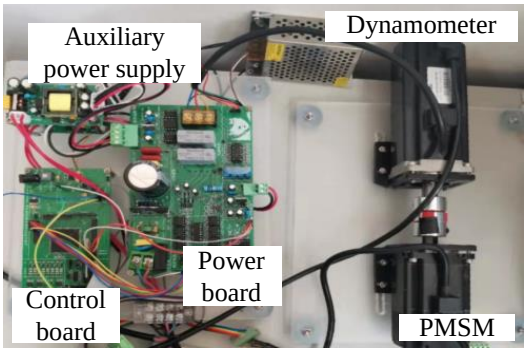

FIGURE 6. Schematic diagram of the experimental platform.

TABLE 1. Parameters of the prototype.

Parameters	Value
Stator resistance R (Ω)	1.6
Inductance L_s (H)	0.005075
Pole Pairs	4
Permanent magnet flux λ_f (Wb)	0.0825
Rated speed n_N (r/min)	3000
Rated power P (kW)	0.2
Rated voltage U (V)	220
Rated current I (A)	2.1
Rated torque T_e (N·m)	0.64

4. EXPERIMENT AND ANALYSIS

In order to verify the effectiveness of the proposed sensorless flux weakening control method, experiments are conducted on the experimental platform shown in Fig. 6 on both the sensorless control algorithm without flux weakening control and the active flux sensorless flux weakening control algorithm. In the experimental platform, the main control unit selected is Texas Instruments' TMS320F28335, and the power drive module uses Mitsubishi's intelligent power module PS21965. The basic parameters of the testing motor are shown in Table 1. Due to the mechanical structure limitations of the encoder, the experimental speed tested is 5500 r/min, and the load torque is rated at 0.64 N·m. The parameters of the speed loop PI controller are $k_p = 0.01$ and $k_i = 0.002$. The parameters of the current loop PI controller are $k_p = 0.2$ and $k_i = 0.73$. The parameters of the PI controller in the voltage closed-loop are set to $k_p = 0.55$ and $k_i = 0.0046$.

The first experiment is conducted on the algorithm without flux weakening control, which used the sensorless control algorithm proposed in Subsection 3.2. The given speed set is 5000 r/min, and the load torque is 0.64 N·m at 0–0.5 s and 0.32 N·m at 0.5–1 s. The corresponding speed waveform, speed error, angle waveform, and angle error waveform are shown in Fig. 7(a). From the figure, it can be seen that when the motor is in this state, the speed error is 50 r/min, and the angle error is -0.78 rad. When the load suddenly changes at 0.5 s, the speed error becomes 300 r/min, and the angle error becomes 0.16 rad. After 0.15 s, it returns to stability, with a speed fluctuation of 50 r/min and an angle error of -0.78 rad. In order to verify the operation effect of the motor under continuous flux weakening, the given speed is increased to 5200 r/min. The corresponding speed waveform, speed error, angle waveform, and angle error waveform are shown in Fig. 7(b). From Fig. 7(b), it can be seen that after reaching 5200 r/min, the system lost control.

Then, the proposed sensorless flux weakening control algorithm experiment is conducted, with a given speed of 5500 r/min and a load torque of 0.64 N·m at 0–0.5 s and 0.32 N·m at 0.5–1 s. The experimental waveform is shown in Fig. 8. From Fig. 8, it can be seen that the motor has a stable operating state at 5500 r/min, with a steady-state speed error of 50 r/min and an angle error of -0.68 rad. When the load suddenly changes at 0.5 s, the speed error becomes 300 r/min, and the angle error becomes 0.21 rad. After 0.03 s, it returns to stability, with a speed fluctuation of 50 r/min and an angle error of -0.62 rad. Compared to Fig. 7(a), the proposed algorithm has a faster speed convergence when the load suddenly changes, the convergence time has been reduced by 80%.

In summary, the proposed sensorless flux weakening control algorithm can ensure that the system does not lose control during the magnetic flux weakening process and that angle error is smaller.

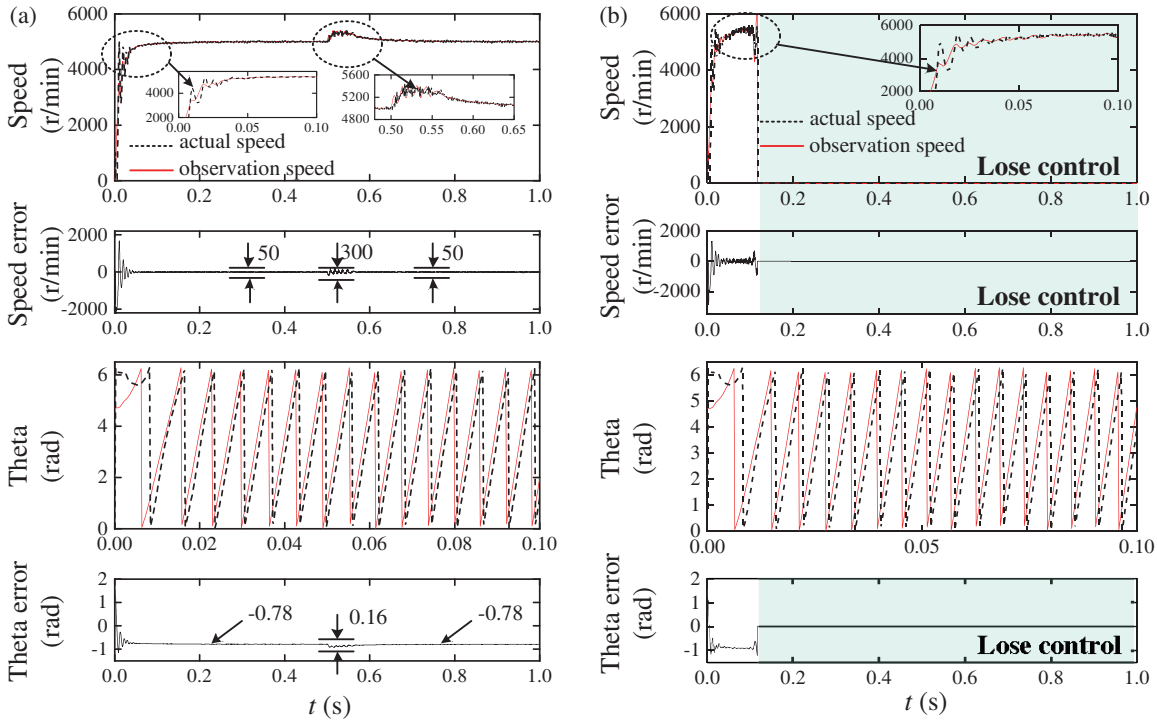

FIGURE 7. Waveforms of the speed sensorless control without flux weakening control algorithm. (a) Case 1. (b) Case 2.

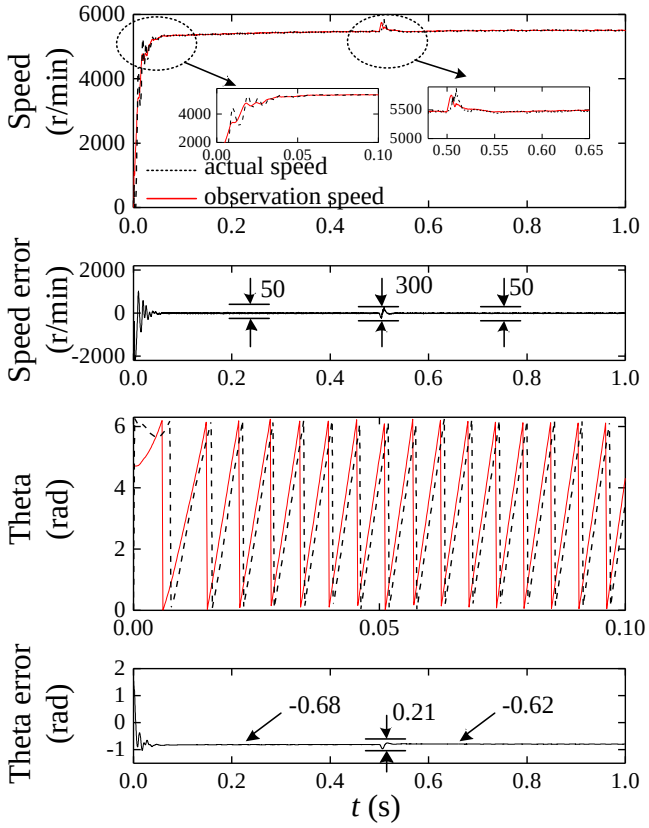

FIGURE 8. Waveforms of the proposed sensorless flux weakening control algorithm.

5. CONCLUSION

A sensorless algorithm based on a voltage closed-loop flux weakening control method is proposed to expand the speed range of PMSM and improve the stability of the control system. The main contributions of this article are: (1) Based on the voltage closed-loop flux weakening control method, the corresponding flux weakening control algorithm has been analyzed and designed. (2) Based on the active flux model, the sliding mode observer and phase-locked loop method are used to observe the speed and rotor position of the motor. (3) Combine the flux weakening control method with the sensorless control method to achieve a sensorless flux weakening control method and improve the stability of the control system.

REFERENCES

[1] Liu, X., Y. Pan, Y. Zhu, H. Han, and L. Ji, "Decoupling control of permanent magnet synchronous motor based on parameter identification of fuzzy least square method," *Progress In Electromagnetics Research M*, Vol. 103, 49–60, 2021.

[2] Zhu, L., B. Xu, and H. Zhu, "Interior permanent magnet synchronous motor dead-time compensation combined with extended kalman and neural network bandpass filter," *Progress In Electromagnetics Research M*, Vol. 98, 193–203, 2020.

[3] Wang, G., M. Valla, and J. Solsona, "Position sensorless permanent magnet synchronous machine drives — A review," *IEEE Transactions on Industrial Electronics*, Vol. 67, No. 7, 5830–5842, 2019.

[4] Xu, D., B. Wang, G. Zhang, G. Wang, and Y. Yu, "A review of sensorless control methods for AC motor drives," *CES Transactions on Electrical Machines and Systems*, Vol. 2, No. 1, 104–115, 2018.

[5] Sun, X., Y. Zhang, X. Tian, J. Cao, and J. Zhu, "Speed sensorless control for IPMSMs using a modified MRAS with gray wolf optimization algorithm," *IEEE Transactions on Transportation Electrification*, Vol. 8, No. 1, 1326–1337, 2022.

[6] Xiao, D., S. Nalakath, S. R. Filho, G. Fang, A. Dong, Y. Sun, J. Wiseman, and A. Emadi, "Universal full-speed sensorless control scheme for interior permanent magnet synchronous motors," *IEEE Transactions on Power Electronics*, Vol. 36, No. 4, 4723–4737, 2020.

[7] Li, C., G. Wang, G. Zhang, N. Zhao, and D. Xu, "Adaptive pseudorandom high-frequency square-wave voltage injection based sensorless control for SynRM drives," *IEEE Transactions on Power Electronics*, Vol. 36, No. 3, 3200–3210, 2020.

[8] Wu, T., D. Luo, X. Wu, K. Liu, S. Huang, and X. Peng, "Square-wave voltage injection based PMSM sensorless control considering time delay at low switching frequency," *IEEE Transactions on Industrial Electronics*, Vol. 69, No. 6, 5525–5535, 2021.

[9] Li, H., X. Zhang, S. Yang, and S. Liu, "Unified graphical model of high-frequency signal injection methods for PMSM sensorless control]," *IEEE Transactions on Industrial Electronics*, Vol. 67, No. 6, 4411–4421, 2019.

[10] Tang, Q., A. Shen, P. Luo, H. Shen, W. Li, and X. He, "IPMSMs sensorless MTPA control based on virtual q-axis inductance by using virtual high-frequency signal injection," *IEEE Transactions on Industrial Electronics*, Vol. 67, No. 1, 136–146, 2019.

[11] Zhang, X., B. Wang, Y. Yu, J. Zhang, and D. Xu, "Overmodulation index optimization method for torque quality improvement in induction motor field-weakening control," *IEEE Transactions on Industrial Electronics*, Vol. 68, No. 12, 11 954–11 967, 2020.

[12] Miguel-Espinar, C., D. Heredero-Peris, G. Gross, M. Llonch-Masachs, and D. Montesinos-Miracle, "Maximum torque per voltage flux-weakening strategy with speed limiter for pmsm drives," *IEEE Transactions on Industrial Electronics*, Vol. 68, No. 10, 9254–9264, 2020.

[13] Deng, T., Z. Su, J. Li, P. Tang, X. Chen, and P. Liu, "Advanced angle field weakening control strategy of permanent magnet synchronous motor," *IEEE Transactions on Vehicular Technology*, Vol. 68, No. 4, 3424–3435, 2019.

[14] Zhang, Z., "Sensorless control of synchronous machines using fundamental back-EMF voltage — A review," *IEEE Transactions on Power Electronics*, 1–1, 2022.

[15] Xu, W., S. Qu, L. Zhao, and H. Zhang, "An improved adaptive sliding mode observer for middle-and high-speed rotor tracking," *IEEE Transactions on Power Electronics*, Vol. 36, No. 1, 1043–1053, 2020.

[16] Volpato Filho, C. J. and R. P. Vieira, "Adaptive full-order observer analysis and design for sensorless interior permanent magnet synchronous motors drives," *IEEE Transactions on Industrial Electronics*, Vol. 68, No. 8, 6527–6536, 2020.

[17] Zuo, Y., C. Lai, and K. L. V. Iyer, "A review of sliding mode observer based sensorless control methods for PMSM drive," *IEEE Transactions on Power Electronics*, Vol. 38, No. 9, 11 352–11 367, 2023.

[18] Boldea, I., M. C. Paicu, and G.-D. Andreescu, "Active flux concept for motion-sensorless unified AC drives," *IEEE Transactions on Power Electronics*, Vol. 23, No. 5, 2612–2618, 2008.

[19] Chen, D., J. Wang, and L. Zhou, "Adaptive second-order active-flux observer for sensorless control of PMSMs with MRAS-based VSI non-linearity compensation," *IEEE Journal of Emerging and Selected Topics in Power Electronics*, Vol. 11, No. 3, 3076–3086, 2023.

[20] Chen, J., J. Mei, X. Yuan, Y. Zuo, and C. H. T. Lee, "Natural speed observer for nonsalient AC motors," *IEEE Transactions on Power Electronics*, Vol. 37, No. 1, 14–20, 2021.

[21] Woldegiorgis, A. T., X. Ge, H. Wang, and M. Hassan, "A new frequency adaptive second-order disturbance observer for sensorless vector control of interior permanent magnet synchronous motor," *IEEE Transactions on Industrial Electronics*, Vol. 68, No. 12, 11 847–11 857, 2020.

[22] Varatharajan, A., G. Pellegrino, E. Armando, and M. Hinkkanen, "Sensorless synchronous motor drives: A review of flux observer-based position estimation schemes using the projection vector framework," *IEEE Transactions on Power Electronics*, Vol. 36, No. 7, 8171–8180, 2021.

[23] Yoo, J., J. Lee, and S.-K. Sul, "Analysis of instability in torque control of sensorless PMSM drives in flux weakening region," *IEEE Transactions on Power Electronics*, Vol. 36, No. 9, 10 815–10 826, 2021.

[24] Ekanayake, S., R. Dutta, F. Rahman, and B. M. Xuan, "Position sensorless control of an interior permanent magnet synchronous machine (IPMSM) in deep flux-weakening region," in *2018 IEEE 9th International Symposium on Sensorless Control For Electrical Drives (SLED)*, 114–119, 2018.